Feeding Network for Sparse-Array Metasurface

Victor Schoofs*, Jonathan Dessy*, David González-Ovejero†, Modeste Bodehou‡, Christophe Craeye*
*(UCLouvain): ICTEAM Institute, Université catholique de Louvain, Louvain-la-Neuve, Belgium, victor.schoofs@uclouvain.be
†(Univ Rennes CNRS): Institut d'Électronique et des Technologies du numéRique (IETR) – UMR 6164, F-35000 Rennes, France
‡(URPHORAN): LETIA/EPAC, Université d'Abomey-Calavi, Abomey-Calavi, Benin

***Abstract*—This paper presents the design of a corporate feeding network (CFN) that enables the generation of a planar surface-wave (SW) wavefront to excite modulated metasurface (MTS) antennas with modulation along a single direction. Specifically, the CFN is adapted for the challenging case of a sparse-array MTS. To meet the unique requirements of this application, a novel design concept was developed with the goal of exciting the MTS using appropriate SWs. The design process considers all stages leading to prototype fabrication, ensuring that practical implementation aspects are fully integrated into the proposed feeding network.**

***Index Terms*—antennas, feeding network, metasurface, surface waves, grating lobes, stripline.**

I. Introduction

A metasurface (MTS) antenna [1] is typically realized using a thin, multi-layered printed circuit board (PCB) with metallic patches periodically arranged on the surface of a dielectric substrate. By varying the dimensions, orientations and shapes of these patches, spatial modulation of the electromagnetic properties can be achieved [2]. This allows the generation of leaky waves (LW) through the interaction between guided/surface waves (SWs) and the patches, thereby enabling manipulation of the antenna radiation pattern, while maintaining a compact, low-profile, and fabrication-friendly antenna architecture suitable for modern high-frequency applications.

In this work, we focus on the specific case of a planar sparse-array MTS designed for one-dimensional (1D) beam scanning. The array elements are spaced at $d = 2\lambda_0$, with λ_0 being the operating wavelength in free space. This paper extends the work presented in [3]. An antenna array is considered sparse when its elements spacing exceeds $\lambda_0/2$. However, such large inter-element spacing introduces grating lobes in the radiation pattern, which degrade directivity by radiating energy into undesired directions. To mitigate these effects, the proposed MTS is designed to exhibit a rectangular embedded element pattern (EEP), which suppresses grating lobes [4]. The developed test structure comprises 7 periods in one direction (x) and is uniformly excited in the orthogonal direction (y). The main objective of this paper is to discuss the challenges associated with designing the feeding network for this structure and to present the developed solution along with its simulation results.

The remainder of this paper is organized as follows. Section II describes the constraints imposed by the sparse-array MTS application and outlines its global structure. Section III details the design of the feeding network. Section IV presents full-wave simulation results obtained using CST [5] and compares them with those obtained from an in-house Method of Moments (MoM) code.

II. Design Requirements and Structure Overview

The MTS array consists of three identical cells, each measuring $2\lambda_0$ along x and $4\lambda_0$ along y, and outlined by a black line in Fig. 1. Its patches are invariant along the y-axis, where the spacing is $\lambda_0/7$, and vary along the x-axis with a spacing of $\lambda_0/12$. Along the x-axis, they can be modeled as a surface impedance with a periodicity of $2/3\ \lambda_0$ [3]. To collimate the beam in the YZ plane, a planar wavefront propagating along the x-axis must be generated so that the patches are uniformly excited along y.

To achieve this, the metasurface is excited by vertical elementary dipoles (VEDs), which are physically implemented as metallic vias. Each MTS cell contains 16 VEDs spaced by $d_{via} = \lambda_0/4$ along the y-axis. This number is chosen to: (i) place the dipoles sufficiently close along y to effectively approximate the effect of a line source with vertical polarization and (ii) match the corporate feeding network, which divides the power by two at each stage. With $2^4 = 16$ outputs, equal power is delivered to all VEDs. A top view of the three-cell array is shown in Fig. 1.

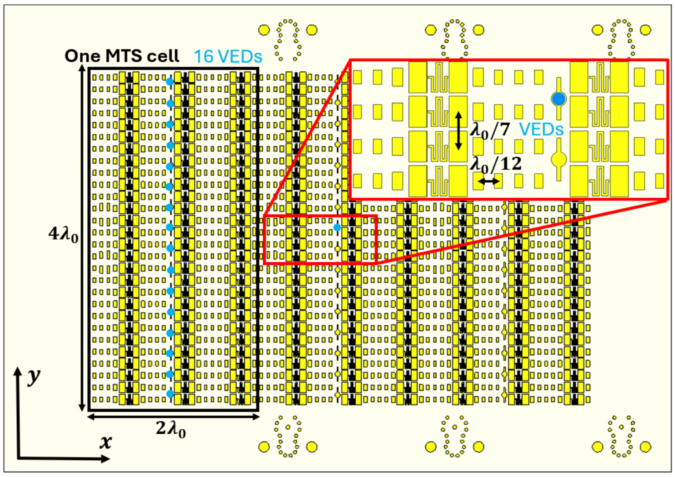

Fig. 1. Top view of the MTS array, composed of three identical cells. Each cell includes its own feeding network terminating in VEDs that generate the planar wavefront. The MTS patches are realized using capacitive impedance elements (squares) and inductive impedance elements (meander lines) [6].

Quarter-wavelength power dividers are a cornerstone of microwave engineering, particularly in array applications, where they are commonly cascaded in corporate feeding networks (CFN). Such dividers have been widely implemented in microstrip, stripline (SLIN), coplanar waveguide (CPW), and even waveguide technologies [7]-[10]. Corporate topologies are favored for their equal power distribution, impedance matching, and predictable phase control. Stripline implementations are particularly suited for dense metasurface environments [11], as they confine fields, limit parasitic coupling with resonant patches, and shield the structure from Radio-Frequency (RF) circuits.

In this work, the feeding network is implemented as a four-stage stripline CFN, at the operating frequency of 24 GHz. This configuration minimizes unwanted coupling to the metasurface patches while ensuring uniform excitation of the VEDs. The CFN stack-up is shown in Fig. 2 and consists of four metallic layers separated by dielectric substrates: two bottom substrates with thickness $h_{sub} = 0.762$ mm, a top substrate with thickness $h_{top} = 1.524$ mm, and copper layers of 35 µm thickness. The substrate used is ROGERS4350b, which has a relative permittivity of $\epsilon_r = 3.66$ and a loss tangent of $tan\ \delta < 0.004$ up to 77 GHz. The stripline network is located in the second layer from the bottom, with the VEDs providing vertical transitions to the patches on the top layer. To reduce simulation time and memory requirements, the results are presented for a three-cell array.

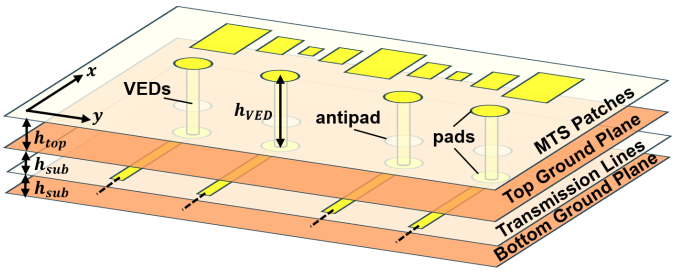

Fig. 2. Schematic of the layer stackup, highlighting key elements including the VEDs wall, pads, and antipads.

III. Feeding Network Design

Considering the constraints discussed above, the resulting feeding network is shown in Fig. 3. Designing such a network is challenging, particularly due to mutual coupling effects, which can lead to strongly uneven current distribution. Each branch of the corporate divider terminates in a VED, which excites SWs. These waves interact and may introduce mismatch and phase imbalances among the VEDs, preventing the formation of a proper planar wavefront. Since the metasurface relies on these SWs for excitation, such effects cannot be entirely avoided and must instead be compensated. Several mitigation strategies were investigated, including adjustments to transmission line length and width, as well as the insertion of matching stubs.

Tapered lines are used to smooth the transition between 50 Ω lines and 100 Ω T-junctions, as shown in Fig. 3,

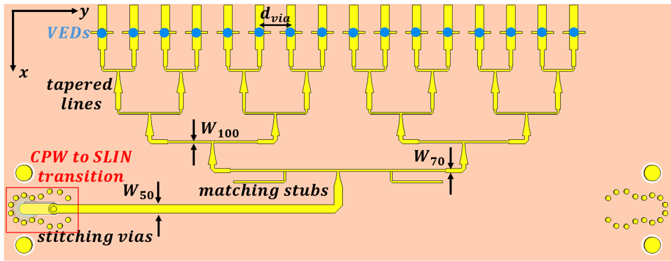

Fig. 3. Top view of the feeding network of one cell of the sparse-array MTS. Highlighted details include matching stubs, tapered lines to reduce T-junction discontinuities, and the CPW-to-stripline transition.

following the techniques reported in [12], [13]. The corporate feeding network itself comprises quarter-wavelength matching lines, each featuring a 70.7 Ω line of length $\lambda_{diel,70}/4$. This length is determined using CST's analytical impedance tool. The key design parameters used in this work are summarized in Table I.

TABLE I
Table of the Variables Used and Their Units

Variable	Symbol	Value	Units
Free-space Wavelength at 24 GHz	λ_0	12.5	mm
Dielectric Wavelength of 70.7 Ω line	$\lambda_{diel,70}$	6.5292	mm
Realtive Permittivity	ϵ_r	3.66	F/m
Width of 50 Ω line	W_{50}	0.85	mm
Width of 70.7 Ω line	W_{70}	0.42	mm
Width of 100 Ω line	W_{100}	0.164	mm
Thickness of the lower dielectric slab	h_{sub}	0.762	mm
Thickness of the top dielectric slab	h_{top}	1.524	mm
Distance between two VEDs	d_{via}	3.125	mm
Height of the VED	h_{VED}	2.321	mm

A. CPW-to-Stripline Transition Design

Feeding the buried SLIN network presented above requires a dedicated transition, as the line is confined between dielectric slabs and ground planes and cannot be directly accessed. To address this, a CPW to SLIN transition was implemented, inspired by the design in [14]. This approach allows the connector to be mounted at the edge of the PCB, avoiding the need to drill through the metasurface patches and thereby preventing additional disruption of the radiating structure. A detailed view of the transition is shown in Fig. 4.

This edge-fed configuration confines the unwanted SWs generated by the central signal via at the edge of the PCB. Such waves could otherwise couple strongly to the VEDs and distort the planar wavefront by introducing magnitude and phase errors. To mitigate this effect, stitching vias (also called via fencing) [15] are positioned around the signal via. These vias act as an electromagnetic shield, confining the fields; they also provide a low-impedance path to the ground planes for the return currents.

Via design is also critical: when the length of a via exceeds $\lambda_0/10$, it begins to behave as a resonant element or a trans-

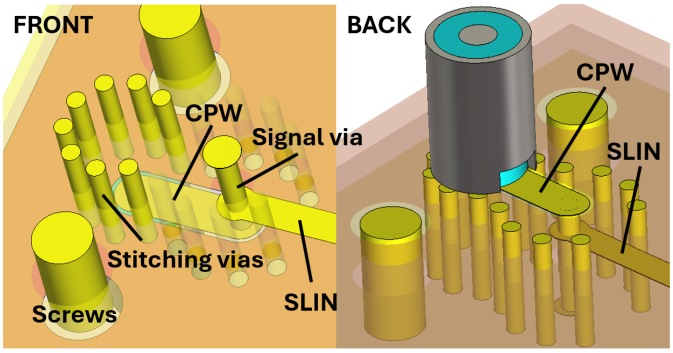

Fig. 4. Front and back views of the CPW–SLIN transition, showing stitching vias and optimized pads for 50 Ω matching.

mission line, potentially introducing mismatch [16]. In this design, the signal via length is close to a quarter-wavelength in free space. Proper 50 Ω matching was achieved by optimizing the pad and antipad radii at each layer of the PCB (see Fig. 2) and carefully arranging the stitching vias. A back-to-back structure was simulated to validate this transition and ensure that the matching does not degrade the performance of the rest of the circuit.

A pressure connector from *SV Microwave* [17] was selected to feed the CPW. It is screwed onto the PCB so that its inner conductor applies direct pressure on the CPW trace, as shown in Fig. 4. This choice allows the MTS to be fed from below the ground plane and provides the flexibility to remove or replace the connector when necessary.

B. Feeding Network Simulation Results

After several optimization iterations, the feeding network was successfully matched over the frequency band of interest, i.e., 23.4–24.4 GHz, as shown in Fig. 5. The reflection coefficient approximately remains below -10 dB across this range. While achieving wideband matching proved challenging, bandwidth was prioritized over perfect return loss, and this level of performance was considered satisfactory.

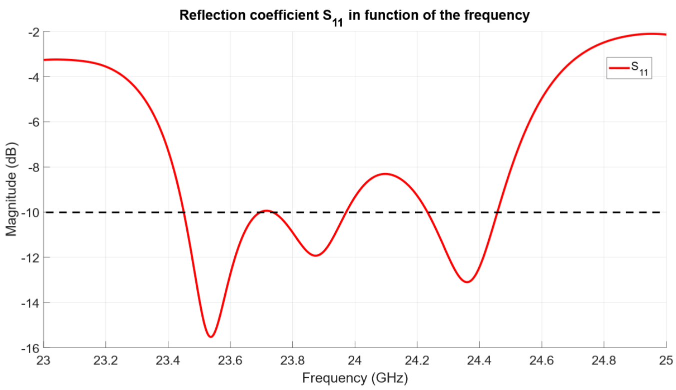

Fig. 5. Reflection coefficient of the MTS as a function of frequency.

Beyond impedance matching, one of the design criteria is the generation of a planar wavefront, which requires that all VEDs support currents of equal magnitude and phase. To evaluate this, lumped ports were inserted into each VED, allowing the extraction of current phase and magnitude. The cuts in the VEDs were kept sufficiently small so as not to affect the impedance during simulation. Fig. 6 reports the phase of the currents in all 16 VEDs, the phase difference remains below 30° at 24 GHz, with a slightly larger deviation observed toward the lower edge of the band.

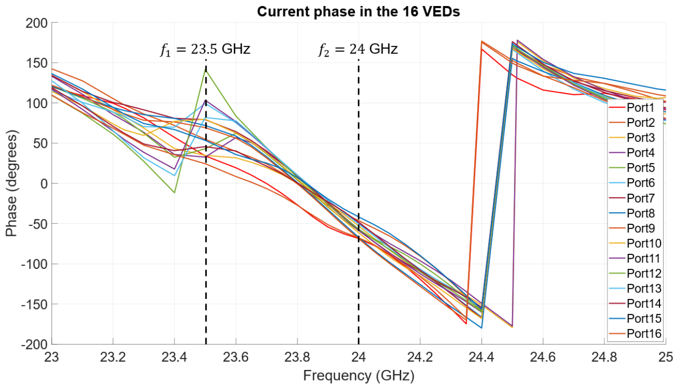

Fig. 6. Phase of the currents in the 16 VEDs, with $f_1 = 23.5$ GHz and $f_2 = 24$ GHz highlighted as examples where the phase uniformity is deemed unacceptable and acceptable, respectively.

Phase uniformity across the VEDs is the most critical factor for planar wavefront generation, even more so than magnitude uniformity. The current magnitude in the lumped elements may vary by as much as 5 dB relative to 1 ampere RMS. As expected from the symmetry of the structure with respect to the x-axis, opposite ports show similar behavior. However, phase deviations remain visible between certain pairs. A maximum phase difference below 30° is considered acceptable. Fig. 7 illustrates how phase differences impact the resulting wavefront by comparing the propagating x-component of the electric field at two frequencies: 24 GHz (see Fig. 7b) where the maximum difference is below 30° and 23.5 GHz where it exceeds this threshold (about 80°, see Fig. 7a), as shown in Fig. 6.

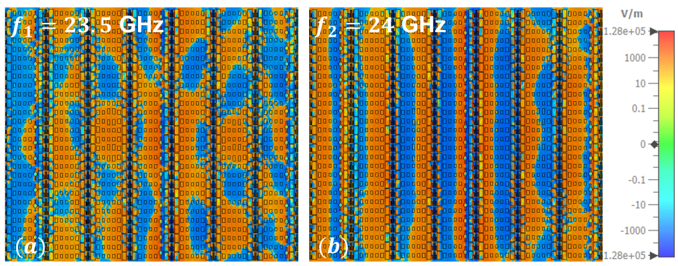

Fig. 7. Comparison of the x-component of the propagating electric field extracted from CST simulations: (a) at 23.5 GHz and (b) at 24 GHz.

At $f_2 = 24$ GHz, the x-component of the electric field forms the desired planar wavefront, whereas at $f_1 = 23.5$ GHz, significant phase mismatches prevent proper SW formation. This highlights the importance of minimizing phase error across all VEDs to ensure consistent metasurface excitation.

IV. Sparse-Array Metasurface Results

The validation criterion before manufacturing this antenna is the radiation pattern obtained when simulating the entire structure. As mentioned in the introduction, the EEP should have a rectangular shape such that it filters out the grating lobes when computing the radiation pattern. Fig. 8 compares EEPs obtained with CST (solid blue line) and with a Method of Moments (MoM) in-house tool [3]. MoM simulations have been conducted for both a 3-cell array (dashed blue line) and a two-dimensional (2D) infinite array of cells along x and y (solid red line).

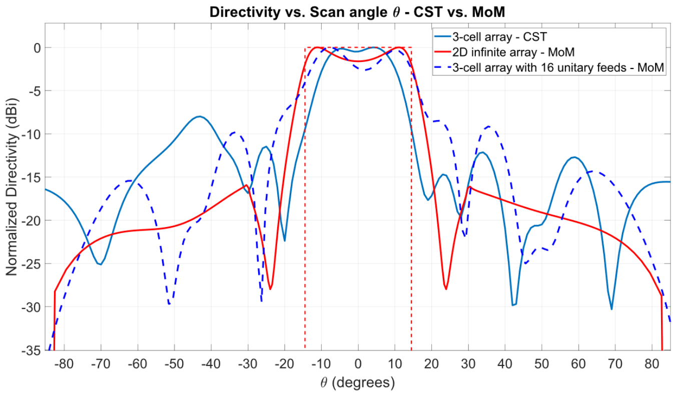

Fig. 8. Comparison between the EEP of 3-cell and infinite arrays using both CST software and MoM at the operating frequency of 24 GHz.

Good agreement is observed between the simulated EEPs. Compared to the objective (dashed red line), the main lobe exhibits a rather sharp rectangular profile, although in CST simulations, while its angular width is narrower than in MoM. The sidelobe level (SLL) also differs slightly, reaching -8 dB in CST compared to -9 dB with MoM. Infinite-array simulations predict significantly lower SLLs, indicating that increasing the number of cells in CST simulations would further reduce sidelobe contributions and bring results closer to the ideal MoM case.

V. Conclusion

A feeding network for a sparse-array metasurface has been designed and validated through full-wave simulations. The proposed structure relies on a four-stage corporate stripline divider that delivers uniform excitation to 16 vertical elementary dipoles (VEDs) per cell, ensuring the generation of a planar surface-wave front. The integration of tapered lines, matching stubs, and a CPW–stripline transition provides satisfactory matching and minimizes parasitic coupling with the metasurface patches. The feeding network had to be carefully optimized to ensure homogeneous phase distribution across the feeding pins, allowing proper planar surface wave excitation.

Simulation results demonstrate satisfactory matching over 23.4–24.4 GHz, with reflection coefficients mostly below -10 dB, and confirm that the feeding network preserves phase uniformity across the VEDs. The resulting radiation patterns show the desired rectangular main lobe and grating lobes suppression, with agreement between CST and MoM models.

These findings validate the proposed feeding concept as a robust candidate for metasurface excitation and the generation of the desired sharp embedded patterns. Future work will focus on fabrication and experimental characterization, as well as extending the approach to larger arrays to further reduce sidelobes.

Acknowledgment

The authors would like to thank Dr. Khaldoun Al Khalifeh from UCLouvain for his advice regarding the CST simulations. Victor Schoofs's activity is funded by the HORIZON EUROPE EIC Pathfinder Open programme under grant agreement No. 101098996 "Flexible intelligent near-field sensing skins (FITNESS)". Funded by the European Union. Views and opinions expressed are however those of the author(s) only and do not necessarily reflect those of the European Union. Neither the European Union nor the granting authority can be held responsible for them. Jonathan Dessy's activity is funded under a Research Fellowship of the Fonds de la Recherche Scientifique - FNRS.

References

[1] S. Maci, G. Minatti, M. Casaletti and M. Bosiljevac, "Metasurfing: Addressing Waves on Impenetrable Metasurfaces," *IEEE Antennas Wireless Propag. Lett.,* vol. 10, pp. 1499-1502, Jan. 2012.

[2] M. A. Francavilla, E. Martini, S. Maci, and G. Vecchi, "On the numerical simulation of metasurfaces with impedance boundary condition integral equations," IEEE Trans. Antennas Propag., vol. 63, no. 5, pp. 2153–2161, May 2015.

[3] J. Dessy, M. Bodehou, J. Cavillot, and C. Craeye "Sparse-array metasurface for beam scanning," *IEEE Trans. Antennas Propag.,* vol. 72, no. 10, pp. 8088–8093, Oct. 2024.

[4] S. P. Skobelev, *Phased Array Antennas With Optimized Element Patterns.* Norwood, MA, USA : Artech House, 2011.

[5] Dassault Systèmes, *CST studio suite 2022,* 2022. [Online]. Available: https: //www.3ds.com/products- services/simulia/products/cst- studiosuite/.

[6] J. Budhu, L. Szymanski, and A. Grbic, "Design of planar and conformal, passive, lossless metasurfaces that beamform," *IEEE J. Microw.,* vol. 2, no. 3, pp. 401–418, Jul. 2022.

[7] A. Abhishek, A. Utsav, R. K. Badhai, and P. Suraj, "Design of Beam Steering Antenna for ISM Band III Using Corporate Feed Network," *Int. Conf. Commun. Electron. Syst. (ICCES),* Coimbatore, India, 2019, pp. 1468-1472.

[8] S. Ogurtsov and S. Koziel, "On Alternative Approaches to Design of Corporate Feeds for Low-Sidelobe Microstrip Linear Arrays," *IEEE Trans. Antennas Propag.,* vol. 66, no. 7, pp. 3781-3786, Jul. 2018.

[9] U. Farooq et al., "Design of a 1×4 CPW Microstrip Antenna Array on PET substrate for Biomedical Applications," *IEEE Int. Symp. Antennas Propag. and USNC-URSI Radio Sci. Meeting,* Atlanta, GA, USA, 2019.

[10] H. Zhao et al., "E-Band Full Corporate-Feed 32 × 32 Slot Array Antenna With Simplified Assembly, *IEEE Antennas Wireless Propag. Lett.,* vol. 20, no. 4, pp. 518-522, Apr. 2021.

[11] Z. Saif, I. Shahid and M. S. Arif, "Implementation of 1×48 stripline feed network for 30 dB first sidelobe level using Taylor aperture distribution," *14th Int. Bhurban Conf. Appl. Sci. Technol. (IBCAST),* Islamabad, Pakistan, 2017, pp. 754-757.

[12] R. S. Sangam, and R. S. Kshetrimayum, "An Improved T-Junction Power Divider Using Linearly Tapered Microstrip Lines," *URSI Asia-Pacific Radio Sci. Conf. (AP-RASC),* New Delhi, India, 2019, pp. 1-4.

[13] L. Liu, S. W. Cheung, and T. I. Yuk, "Compact mimo antenna for portable uwb applications with band-notched characteristic," *IEEE Trans. Antennas Propag.,* vol. 63, no. 5, pp. 1917–1924, May 2015.

[14] M. Leib, M. Mirbach, and W. Menzel, "An ultra-wideband vertical transition from microstrip to stripline in PCB technology," *IEEE Int. Conf. on Ultra-Wideband,* Nanjing, China, 2010, pp. 1-4.

[15] D. Li, J. Xu, B. Zhang, W. Liu and L. Du, "GCPW to stripline vertical transition for K-band applications in LTCC," *Asia-Pacific Microw. Conf. (APMC),* Nanjing, China, 2015.

[16] T. Kushta, K. Narita, T. Kaneko, T. Saeki and H. Tohya, "Resonance stub effect in a transition from a through via hole to a stripline in multilayer PCBs," *IEEE Microw. and Wireless Compon. Lett.,* vol. 13, no. 5, pp. 169-171, May 2003.

[17] "2.92 mm Female Solderless LiteTouch PCB Connector, 2 Hole (CPW / Microstrip), SF1521-60115," SV Microwave. [Online]. Available: https://www.svmicrowave.com/292mm-female-solderless-litetouch-pcb-connector-2-hole-cpw-microstrip. "Accessed: Oct. 3, 2025."